

Optimization of adsorption parameters for Fe (III) ions removal from aqueous solutions by transition metal oxide nanocomposite

Narges Samadani Langeroodi, Zhaleh Farhadraresh & Aliakbar Dehno Khalaji

To cite this article: Narges Samadani Langeroodi, Zhaleh Farhadraresh & Aliakbar Dehno Khalaji (2018) Optimization of adsorption parameters for Fe (III) ions removal from aqueous solutions by transition metal oxide nanocomposite, Green Chemistry Letters and Reviews, 11:4, 404-413, DOI: 10.1080/17518253.2018.1526329

To link to this article: <https://doi.org/10.1080/17518253.2018.1526329>



© 2018 The Author(s). Published by Informa UK Limited, trading as Taylor & Francis Group



Published online: 03 Oct 2018.



Submit your article to this journal [↗](#)



Article views: 1349



View related articles [↗](#)



View Crossmark data [↗](#)



Citing articles: 10 View citing articles [↗](#)

Optimization of adsorption parameters for Fe (III) ions removal from aqueous solutions by transition metal oxide nanocomposite

Narges Samadani Langeroodi, Zhaleh Farhadraresh and Aliakbar Dehno Khalaji

Faculty of Science, Department of Chemistry, Golestan University, Gorgan, Iran

ABSTRACT

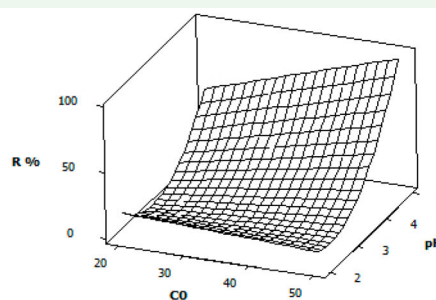
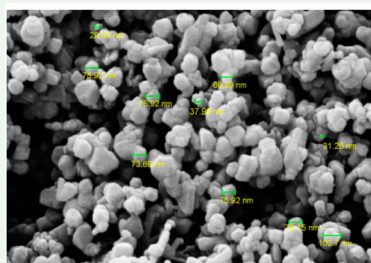
Manganese oxide nanocomposite (Mn_2O_3/Mn_3O_4) was prepared by sol-gel technique and used as an adsorbent. Fourier Transform Infrared (FTIR) spectroscopy, X-ray diffraction (XRD), and Field Emission Scanning Electron Microscopy (FE-SEM) were used to characterize the adsorbent. The response surface methodology (RSM) was employed to evaluate the effects of solution pH, initial Fe (III) ions concentration, adsorbent weight, and contact time on the removal ratio of the Fe (III) ions. A total of 27 adsorption experimental runs were carried out employing the detailed conditions designed based on the Box-Behnken design (BBD). Results showed that the pH of the solution and initial Fe (III) ions concentration were the most significant parameters for Fe (III) ions removal. In process optimization, the maximal value of the removal ratio of Fe (III) was achieved as 95.80%. Moreover, the corresponding optimal parameters of adsorption process were as: contact time = 62.5 min, initial Fe (III) concentration = 50 mg/L, adsorbent weight = 0.5 g, and pH = 5. The experimental confirmation tests showed a strong correlation between the predicted and experimental responses ($R^2 = 0.9803$). The fitness of equilibrium data to common isotherm equations such as Langmuir, Freundlich, and Temkin were also tested. The sorption isotherm of adsorbent was best described by the Langmuir model. The kinetic data were analyzed using pseudo-first-order, pseudo-second-order, intraparticle diffusion, and Elovich kinetic models. The adsorption kinetics of Fe (III) ions were well fitted with the pseudo-second-order kinetic model.

ARTICLE HISTORY

Received 3 January 2018
Accepted 17 September 2018

KEYWORDS

Nanocomposite; adsorption; response surface; equilibrium isotherms; kinetics



1. Introduction

Today, adsorption is used as one of the most promising methods in removal process of heavy metal ions because of its high efficiency, easy handling, and the effectiveness of various adsorbents (1, 2). Liquid-solid adsorption systems are based on the ability of certain solids to preferentially concentrate specific substances from solutions onto their surfaces. Metal oxide nanoparticles, often characterized by a significant amount of surfaces and high capacity, are among the promising adsorbents for heavy metals removal because of their unique properties and potential applications (3–5). It is well known

that heavy metals have toxic or harmful effects on many forms of life. Iron in the environment enters to water through from steel tempering, coal coking, and mining industries (6, 7). Iron toxicity can cause anorexia, shock, and oliguria. Iron overdose known as hemochromatosis is caused by a gene that enhances iron absorption in the body (8). Iron accumulates over time in the liver, bone marrow, pancreas, skin, and testicles. Accumulation of iron in these organs causes them to functions poorly (9, 10).

The aim of this work is the synthesis of manganese oxide nanocomposite (Mn_2O_3/Mn_3O_4) and its application

CONTACT Narges Samadani Langeroodi  n.samadani@gu.ac.ir, nsamadani@yahoo.com

© 2018 The Author(s). Published by Informa UK Limited, trading as Taylor & Francis Group
This is an Open Access article distributed under the terms of the Creative Commons Attribution License (<http://creativecommons.org/licenses/by/4.0/>), which permits unrestricted use, distribution, and reproduction in any medium, provided the original work is properly cited.

for adsorption of Fe (III) ions. Nanoparticles were synthesized by sol-gel method and characterized by IR, SEM, and XRD. The important parameters that affect the adsorption were explored using the response surface methodology approach (RSM). RSM is a statistical and graphical technique that is useful in studying the interactions of two or more factors affecting the adsorption process and determining the optimum operating conditions for the system (11–14). The Box-Behnken design (BBD) of the RSM was employed to investigate the effects of significant factors that influenced the removal of Fe (III) ions from aqueous solution by $\text{Mn}_2\text{O}_3/\text{Mn}_3\text{O}_4$ nanocomposite and understand their impact on the process. Langmuir isotherm model was applied to fit equilibrium sorption data. The experimental data were analyzed using the pseudo-first-order, pseudo-second-order, intraparticle diffusion, and Elovich kinetic models.

2. Experimental section

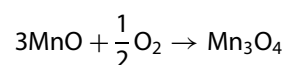
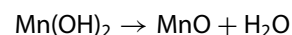
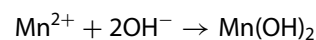
2.1. Materials and methods

The chemicals used during this study such as Fe $(\text{NO}_3)_3 \cdot 9\text{H}_2\text{O}$, Mn $(\text{NO}_3)_2 \cdot 4\text{H}_2\text{O}$, NaOH, and HCl were purchased from the Merck and used as received without further purifications. The Fourier transform infrared (FTIR) analysis of the metal oxides used in this study was characterized by an FTIR apparatus (Perkin-Elmer Model System 2000 using KBr pellet method). In order to directly observe the surface morphology of the adsorbent, Field emission scanning electron microscopy (FE-SEM) (SIGMA VP-500, Germany) was employed in this study. The elemental information and structure of synthesized material were determined by an X-ray diffractometer (XRD) (X'Pert Pro, Analytical, Netherlands) at ambient temperature. N_2 adsorption-desorption isotherm and the specific surface area of the particle were carried out on a Brunauer-Emmett-Teller (BET) surface area analyzer (Nova Station A, Quantachrome, America) for nitrogen adsorption. Fe (III) remaining unadsorbed in the supernatant liquid was determined with an Atomic Absorption Spectrometer (model Shimadzu, AA-7000).

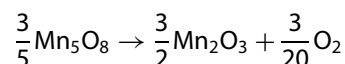
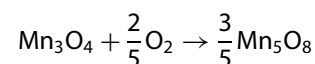
2.2. Preparation of nanocomposite

In the laboratory, the manganese oxide nanocomposite was prepared by sol-gel method. First, 5 g desired metal salt ($\text{Mn}(\text{NO}_3)_2 \cdot 4\text{H}_2\text{O}$) was dissolved in 75 mL deionized water. Then, 1 M NaOH solution was added dropwise to the above mixture through the mechanical stirring at room temperature. When pH reached 13, the

stirrer was turned off and the obtained solution was kept at room temperature for 24 h. After this time, the content was filtered off and washed several times to remove any NaOH with deionized water and the wet powders were dried at 70° for 18 h. The obtained dry powder was heated in a quartz tube furnace at 250° for 3 h and, finally, was calcinated at 600° for 3 h. Manganese ions were first reduced in alkaline aqueous to $\text{Mn}(\text{OH})_2$ and then decomposed into MnO. Eventually, MnO was oxidized to Mn_3O_4 at 250° (15, 16):



As confirmed by earlier studies (17, 18), in the temperature range of $300\text{--}450^\circ$, Mn_3O_4 (Mn_1^{2+} , Mn_2^{3+}) can be transformed into Mn_5O_8 (Mn_2^{2+} , Mn_3^{4+}). Next, Mn_5O_8 was reduced to Mn_2O_3 at 600° . The reactions scheme can be written as follows:



N_2 adsorption-desorption isotherm of manganese oxide nanocomposite is presented in Figure 1 and the corresponding physicochemical properties including BET surface and average pore volume are shown in Table 1.

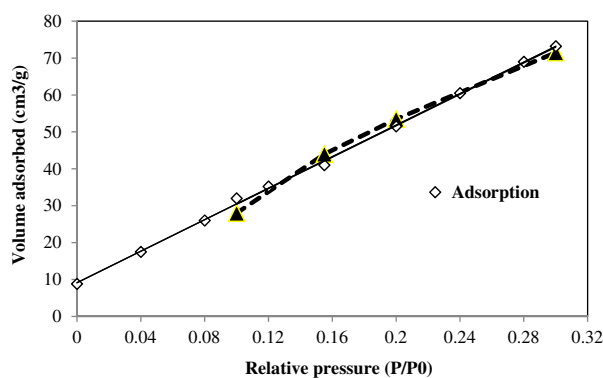


Figure 1. N_2 adsorption-desorption isotherm of manganese oxide nanocomposite.

Table 1. Textural properties of manganese oxide nanocomposite.

BET surface area (m^2/g)	Average pore volume (cm^3/g)
15.53	0.125

2.3. Adsorption experiments

Adsorption experiments were performed by mixing a certain amount of adsorbent with 200 mL of the heavy metal solution of known pH and initial concentration. The suspensions were equilibrated by shaking for a desired period of time. The clear supernatants after filtration were analyzed for Fe (III) ions concentration using an atomic absorption spectrometer. The removal ratio of metal ions was calculated using the following equation:

$$\eta = \frac{C_0 - C_e}{C_0} \times 100\% \quad (1)$$

where C_0 (mg/L) and C_e (mg/L) are the initial and equilibrium concentrations of the adsorbate, respectively, and η is the removal ratio (in percent) of Fe (III) ions.

The amount of Fe (III) adsorbed per unit of adsorbent, q_t (mg/g), was calculated according to mass balance on the iron concentration; Equation (2):

$$q_t = \frac{(C_0 - C_t)V}{W} \quad (2)$$

where V (L) is the volume of the solution, W (g) is the weight of adsorbent, and C_t (mg/L) is the concentration of the adsorbate at time t .

2.4. Design of experiments

Box-Behnken Design is one of the most efficient experimental designs among of other response surface designs, because of its ability to estimate the parameters of the quadratic polynomial model and detection of lack of fit of the model (19). A 3-level, 4-factor Box-Behnken Design was used to evaluate the effect of the selected parameters on the removal efficiency of Fe (III) ions from water by the adsorbent. Four parameters affecting heavy metal removal, namely solution pH (X_1), initial Fe (III) concentration (X_2), adsorbent weight (X_3), and contact time (X_4) were selected as independent variables, and the removal ratio (Y) of Fe (III) ions were considered as the dependent variable (the predicted response) (Table 2).

Table 2. Experimental range and coded levels of independent variables.

Independent variables	Low coded (-1)	Middle coded (0)	High coded (+1)
Initial Fe (III) concentration, X_1 (mg/L)	20	35	50
pH, X_2	2	3.5	5
Adsorbent weight, X_3 (g)	0.1	0.5	0.9
Contact time, X_4 (min)	5	62.5	120

A regression quadratic polynomial model is described in Equation (3):

$$R(\%) = \alpha_0 + \sum \alpha_i X_i + \sum \alpha_{ij} X_i^2 + \sum \alpha_{ij} X_i X_j + \varepsilon \quad (3)$$

Where α_0 is the constant coefficient, α_i , α_{ij} , and α_{ij} are the regression coefficients and X_i and X_j indicate the independent variables. Moreover, ε represents the random error (20).

3. Results and discussion

3.1. Effects of adsorbent weight and initial concentration at fixed contact time and pH

Adsorbent weight studies were carried out at room temperature, a pH of 3, and a fixed time (180 min) for two different adsorbate concentrations (minimum and maximum adsorbate concentrations 20 and 50 mg/L, respectively). It could be seen from the Figure 2 that the removal ratio increased gradually with increasing adsorbent weight to a maximum 0.9 g. After this maximum equilibrium value, the removal ratio did not increase with increasing adsorbent weight. These results suggest that the relationship between adsorbent weight and removal ratio was related to the increase in the number of adsorption sites and that increasing this number had no effect after equilibrium was reached. From the results, the minimum and maximum weights of adsorbent were determined as 0.1 g and 0.9 g, respectively. Figure 2 represents that sufficient adsorption sites are available at lower initial concentration, but at higher concentration, metal ions are greater than adsorption sites.

3.2. Effects of contact time and initial concentration at the fixed adsorbent weight and pH

Figure 3 represents the effects of contact time on the removal ratio of Fe (III) ions under different initial

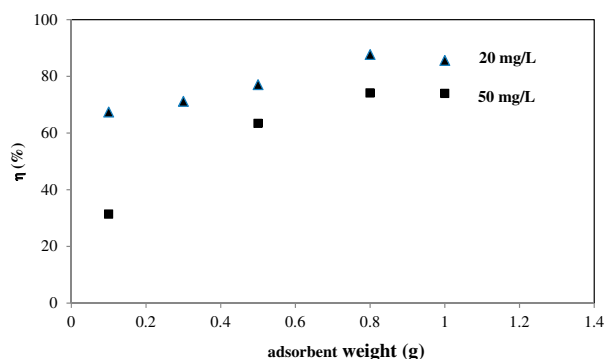


Figure 2. Effects of adsorbent weight and initial concentration for minimum and maximum concentrations of 20 and 50 mg/L, respectively, on removal ratio of Fe (III) ions at room temperature, pH = 3, and $t = 180$ min.

concentrations. As can be noticed, the removal ratio of Fe (III) ions increases with contact time and finally reaches an equilibrium state in approximately 120 min. From the results, the minimum and maximum contact times were determined as 5 and 120 min, respectively.

Contact time studies show that an increase in the concentration initial Fe (III) ions results in a decrease in the removal ratio. This result can be attributed to the fact that for a fixed adsorbent weight, the total available adsorption sites are limited. Thus, due to saturation of the adsorbate into the adsorbent and less of binding sites, with increasing initial Fe (III) ions concentration the removal ratio decreases.

3.3. Effect of pH at fixed contact time and adsorbent weight

Effect of pH on the adsorption of Fe (III) ions was investigated at different pH values ranging from 2.0 to 5.0 (Figure 4). The pH of the solution affects the surface charge of adsorbent. At low pH, H_3O^+ ions were adsorbed on the surface of adsorbent so that the net charge of adsorbent was positive and the removal ratio of Fe (III) was low. At higher pH, the adsorption of Fe (III) ions occurred through a co-operation of ion exchange and electrostatic interaction. Maximum adsorption was observed at about pH 3. With increasing pH values (up to 5) the adsorbent surface becomes more negative. Therefore, negatively charged Fe (III) species may be repelled by the negatively charged adsorbent surface functional groups, which result in a decrease in the removal ratio of Fe (III). At pH values higher than 5, Fe (III) precipitation occurred. Therefore, pH values higher than 5 were not investigated. In general, the results indicated that adsorption is highly pH dependent. Similar results were reported in the literature (3).

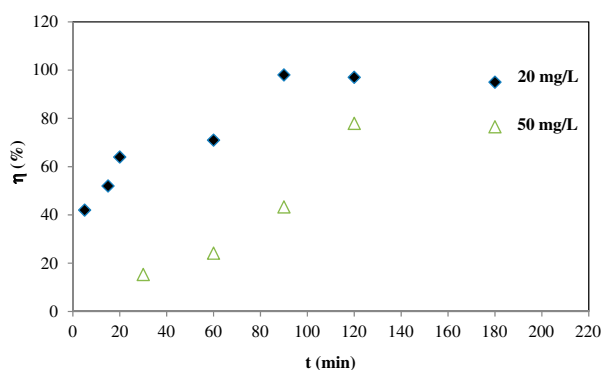


Figure 3. Effects of contact time and initial concentration on the removal ratio of Fe (III) ions at room temperature, pH = 3, and adsorbent weight = 0.9 g.

3.4. FT-IR spectroscopy

The FT-IR spectra of manganese oxide (Mn_2O_3/Mn_3O_4) nanocomposite is shown in Figure 5. In the IR spectra of Mn_2O_3/Mn_3O_4 , the stretching vibration bands located at 588 cm^{-1} correspond to the vibration of Mn-O in an octahedral environment, while the stretching vibration band located at 484 cm^{-1} can be attributed to the vibration of manganese species ($Mn^{3+}-O$) in the octahedral site of Mn_3O_4 . The stretching vibration band at 484 cm^{-1} confirmed the Mn_2O_3 (16, 21). Two weak absorption bands at 1450 and 1630 cm^{-1} are attributed to the water molecules adsorbed on the surface of nanoparticles.

3.5. X-ray diffraction (XRD)

The crystalline structure of this nanoparticle was characterized by XRD. XRD patterns of manganese oxide nanocomposite (Mn_2O_3/Mn_3O_4) are shown in Figure 6. The average crystallite sizes was calculated from the XRD line broadening using the Scherrer's formula ($d = 0.9 \lambda / \beta \cos\theta$), where d is the crystallite size (nm), θ is the angle of incidence, λ is the wavelength of x-ray diffraction ($\lambda = 1.5406\text{ nm}$), and β is the full width at half maximum (22). The average crystallite sizes of the nanoparticle are about 48 nm measured from the peak appears at $2\theta = 38.41^\circ$ using the Debye Scherrer approximation. From Figure 5, the peak positions at $2\theta = 23.33, 33.14, 38.41, 45.34, 49.53, 55.35,$ and 65.93° confirmed the preparation of Mn_2O_3/Mn_3O_4 nanocomposite with a cubic structure, which is in accordance with those of the standard spectrum (No. 41-1442 and 24-0734). XRD results showed that the prepared nanoparticle is a well-crystalline material.

3.6. FE-SEM imaging of the adsorbent

The morphology and the nature of the surface of adsorbent are presented by the FE-SEM image (Figure 7). The

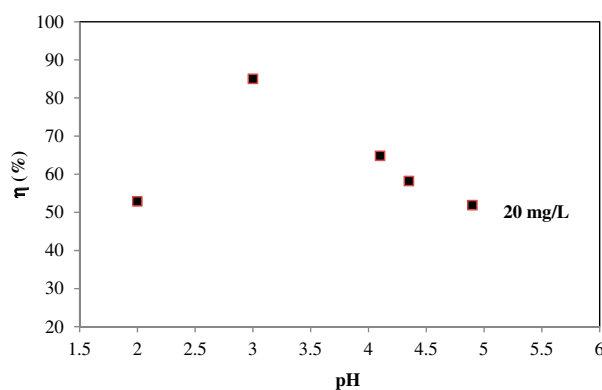


Figure 4. Effect of pH on the removal ratio of Fe (III) ions at room temperature, adsorbent weight = 0.9 g, and $t = 120$ min.

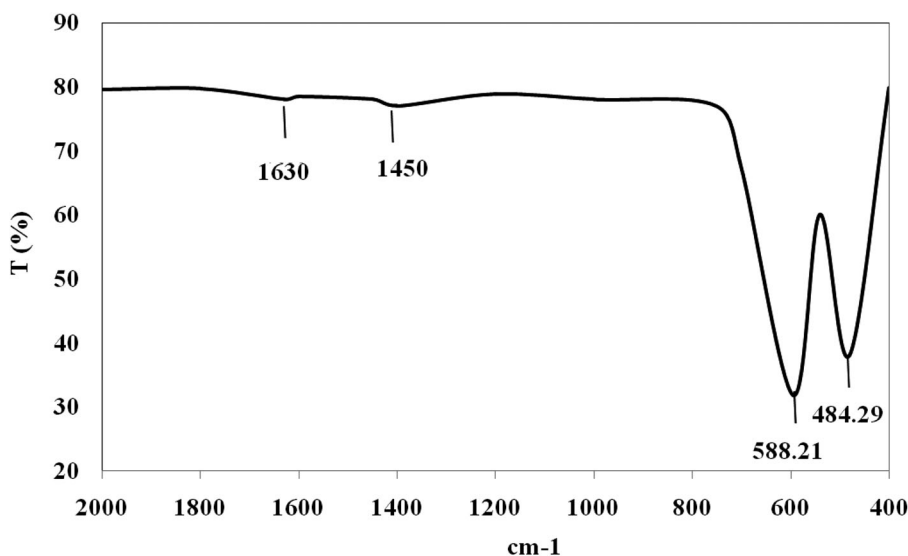


Figure 5. FT-IR spectra of $\text{Mn}_2\text{O}_3/\text{Mn}_3\text{O}_4$ nanocomposite.

FE-SEM image of $\text{Mn}_2\text{O}_3/\text{Mn}_3\text{O}_4$ nanocomposite shows several hundreds of nanoparticles. Aggregated nanoparticles with a diameter varying between 30 and 80 nm are observed in this figure. The FE-SEM image of $\text{Mn}_2\text{O}_3/\text{Mn}_3\text{O}_4$ nanocomposite confirmed the spherical or approximately spherical morphology of nanoparticles with a porous surface, which may be beneficial to metal ions diffusion and adsorption.

A microstructure measurement software was employed to determine mean diameter and statistical distribution of particle size by FE-SEM image (Figure 8).

The mean diameters determined by FE-SEM and XRD are in good agreement.

3.7. Fitting model

The experimental values for each independent variable were chosen according to the results obtained from

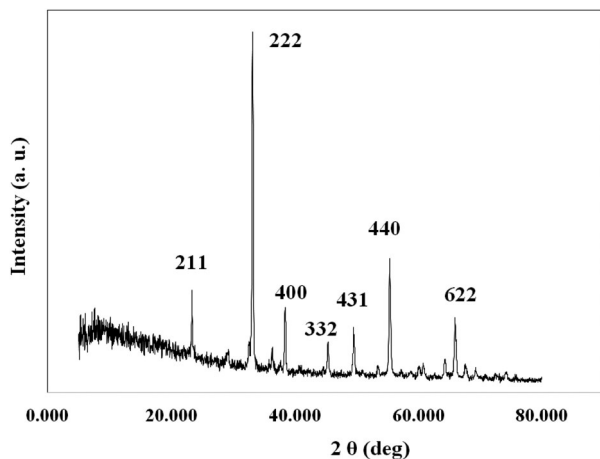


Figure 6. XRD patterns of $\text{Mn}_2\text{O}_3/\text{Mn}_3\text{O}_4$ nanocomposite.

the preliminary analysis. The coded levels of independent variables (-1, 0, 1 for low, middle, and high values) and response values (removal ratio) based on the Box-Behnken Design using MINITAB software are shown in Table 3.

A model that demonstrates the relationship between Fe (III) ions removal ratio and independent variables is given in Equation (4). The model is proposed based on the regression coefficients.

$$Y = 158.2 - 1.405A - 94.9B + 13.45B^2 + 0.585AB \quad (4)$$

where Y is the predicted responses for the removal ratio of Fe (III) and A and B are the initial Fe (III) concentration and pH. The predicted value of removal ratio of Fe (III) obtained using Equation (4), i.e. 95.80, is close to the experimental value, i.e. 92.60, providing that the model is fully applicable. The results of analysis of variance (ANOVA) for the removal ratio of Fe (III) are shown in Table 4. The larger the value of F (41.31) and the smaller

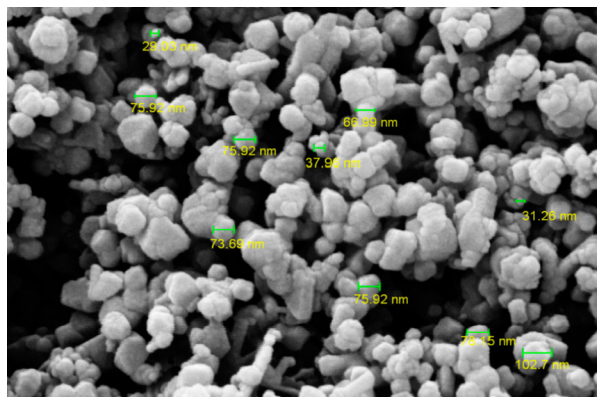


Figure 7. FE-SEM of adsorbent.

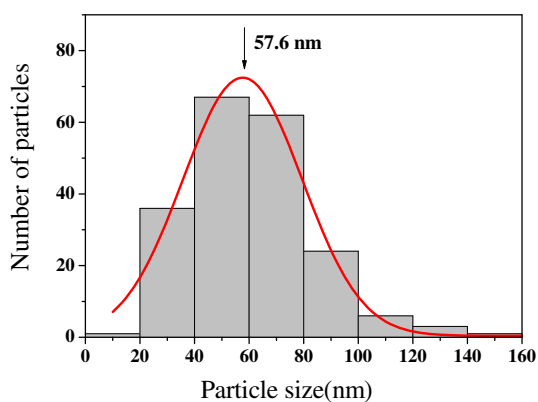


Figure 8. Particle size distribution of adsorbent by FE-SEM.

the value of P (<0.05) the more significant is the corresponding coefficient term (23). As can be seen from Table 3, all the p -values of A, B, B^2 , and AB are less than

0.05, suggesting that these variables are significant on the removal of Fe (III) ions. As shown in Table 2, the R^2 value of 88.25 for Fe (III) ions removal model showed the almost well fitness of regression model for predicting the removal results. The close correspondence between R_{adj}^2 and R^2 indicates that unnecessary variables have not been included. The ANOVA results showed that the pH of the solution and initial Fe (III) concentration were the most significant parameters for Fe (III) ions removal.

3.8. Determination of model adequacy

One of the key assumptions for the statistical analysis of data from experiments is that the data come from a normal distribution. Figure 9 represents predicted vs. actual values of removal ratio of Fe (III). The clustering of the points around the straight line indicates a good relationship between the experimental (actual) and the

Table 3. Box-Behnken design matrix for four variables and response values.

Experimental run	Initial Fe (III) concentration (A)	pH (B)	Adsorbent weight (C)	Contact time (D)	Removal ratio (%)
1	0	0	-1	1	16.85
2	-1	-1	0	0	15.75
3	1	0	-1	0	25.10
4	0	0	-1	-1	7.78
5	0	-1	-1	0	7.85
6	1	-1	0	0	14.68
7	1	0	1	0	23.66
8	-1	0	1	0	0.00
9	-1	0	-1	0	0.00
10	-1	0	0	-1	0.00
11	0	0	0	0	7.85
12	-1	0	0	1	16.25
13	-1	1	0	0	41.00
14	0	0	0	0	14.90
15	0	-1	1	0	21.52
16	0	1	0	-1	52.85
17	0	1	0	1	63.03
18	0	0	0	0	22.85
19	0	-1	0	-1	0.00
20	0	-1	0	1	23.39
21	0	1	1	0	94.28
22	1	0	0	1	21.5
23	0	0	1	1	10.53
24	0	0	1	-1	18.92
25	1	0	0	-1	11.18
26	0	1	-1	0	94.17
27	1	1	0	0	92.60

Table 4. ANOVA results for optimization of Fe (III) ions adsorption.

Source	Degree of freedom (DF)	Coefficient estimate	Sum of squares (SS)	Mean square (MS)	F-value	p-Value
Model	4	158.2	18404.1	4601.0	41.31	0.000
A	1	-1.405	1115.9	1115.9	10.02	0.004
B	1	-94.9	10486.7	10486.7	94.16	0.000
B^2	1	13.45	6107.9	6107.9	54.84	0.000
AB	1	0.585	693.5	693.5	6.23	0.021
Residual error	21		2450.3	111.4		
Lack of fit	19		2337.6	116.9	2.08	0.375
Pure error	2		112.6	56.3		
Total	26		20854.4			

$R^2 = 88.25$.

$R_{pred}^2 = 82.04$.

$R_{adj}^2 = 86.11$.

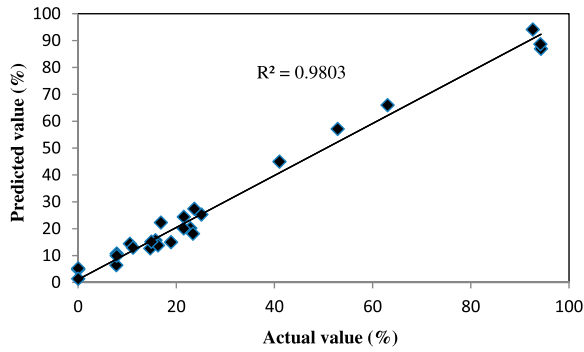
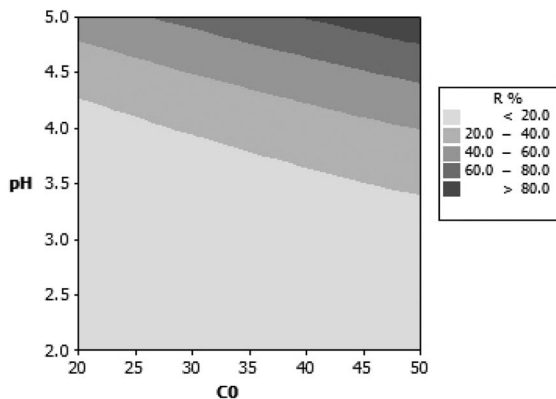


Figure 9. Predicted vs. actual values of removal ratio of Fe (III).

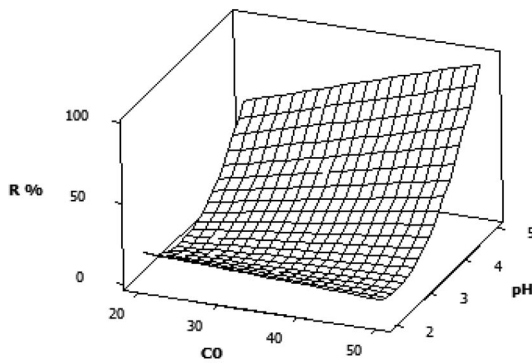
prediction values, confirming the robustness of the model.

3.9. Contour plot and response surfaces

Figure 10(a) shows a contour plot of the relationship between initial Fe (III) concentration and pH. It can be seen that at upper values of C_0 , maximum removal ratio occurs at higher values of pH. Therefore, there is



(a)



(b)

Figure 10. (a) Contour plots and (b) response surface for Fe (III) ions adsorption at adsorbent weight = 0.5 g and contact time = 62.5 min.

an optimum at upper values of C_0 and higher values of pH. The optimized conditions of the process determined by the software are pH = 5, initial adsorbate concentration = 50 mg/L, adsorbent weight = 0.5 g, and contact time = 62.5 min for a maximum removal ratio of 95.80%. The interaction between initial Fe (III) concentration and pH is presented by response surface plot Figure 10(b). Response surfaces plots, obtained as a function of two factors maintaining all other factors constant, are helpful in understanding both the main effects and the interaction effects of these two factors (19, 24). It could be seen that an increase in pH value from 2 to 5 resulted in enhancing the removal ratio of Fe (III) ions from 10.5% to 95%. Therefore, pH of solution played an important role in the removal ratio of Fe (III) ions on adsorbent as was evident from the equation (coefficients in Equation 4) and plot.

3.10. Adsorption equilibrium isotherm

Adsorption isotherm describes how the metal ions are distributed between the liquid and solid phases when the adsorption process reaches an equilibrium state, as their distribution manner is an important factor in determining the maximum sorption capacity.

3.10.1. Langmuir isotherm model

The linear equation of Langmuir isotherm model is expressed as follows:

$$\frac{C_e}{q_e} = \frac{C_e}{q_m} + \frac{1}{K_L q_m} \quad (5)$$

where q_m is the monolayer adsorption capacity of adsorbent (mg/g) and K_L is the Langmuir adsorption constant related to the energy of adsorption (L/mg) (25); Figure 11 and Table 5.

3.10.2. Freundlich isotherm model

The Freundlich equation is an empirical equation that is very useful as it accurately describes much adsorption

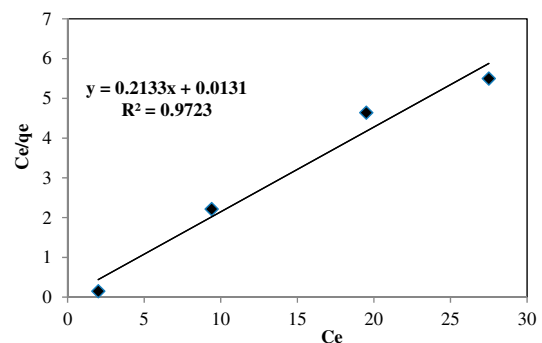


Figure 11. Isotherm plot for the adsorption of Fe (III).

Table 5. Langmuir, Freundlich, and Temkin constants.

	Langmuir
q_m (mg/g)	22.03
K_L (L/mg)	0.897
r^2	0.981
Δq_t (%)	0.052
	Freundlich
n_F	1.993
K_F ((mg/g) · (L/mg) ^{1/n})	8.84
r^2	0.961
Δq_t (%)	0.12
	Temkin
B_T	4.947
K_T (L/mg)	8.32
r^2	0.966
Δq_t (%)	0.078

data. The Freundlich isotherm (Van Bemmelen equation) is in the linearized form

$$\log q_e = \log K_F + \frac{1}{n} \log C_e \quad (6)$$

where K_F and n are Freundlich constants concerning the multilayer adsorption capacity and adsorption intensity, respectively (Table 5).

3.10.3. Temkin isotherm model

Temkin and Pyzhev (1940) considered the effect of the adsorbate interaction on adsorption and proposed the model known as the Temkin isotherm, which can be expressed as:

$$q_e = B_T \ln K_T + B_T \ln C_e$$

$$B_T = \frac{RT}{b} \quad (7)$$

Where K_T (L/mg) is Temkin isotherm energy constant, B_T is Temkin isotherm constant related to the heat of sorption, R is the gas constant, and T is the temperature (Table 5).

It can be vividly seen from these results that the coefficients of determination (R^2) were very high for three models above. The applicability of the three models to describe the adsorption process was further validated by the normalized standard deviation, Δq_t (%), which is defined as:

$$\Delta q_t (\%) = \sqrt{\frac{\sum [(q_{t,exp} - q_{t,cal})/q_{t,exp}]^2}{N - 1}} \quad (8)$$

where N is the number of data points and $q_{t,exp}$ and $q_{t,cal}$ (mg/g) are the experimental and calculated adsorption capacity, respectively. Based on the highest R^2 values and the lowest Δq_t values, the Langmuir model was, therefore, the most suitable equation to describe the adsorption isotherms of Fe (III) on Mn_2O_3/Mn_3O_4 nano-composite prepared (Table 5).

3.11. Adsorption kinetics

Except for adsorption capacity, the kinetic performance of a given adsorbent is the base to determine the performance of fixed-bed or any other flow-through systems (26). Kinetic studies show the uptake rate of adsorbate, which controls the resident time of the whole adsorption process. The applicability of the pseudo-first-order (27), pseudo-second-order (28), intraparticle diffusion (29), and Elovich (30) models were tested for the adsorption of Fe (III) ions onto the adsorbent. Adsorption kinetics was studied by varying the time of reaction in an optimal amount of parameters.

3.11.1. The Pseudo-first-order kinetic model

The Lagergren rate equation is one of the most widely used adsorption rate equations for the adsorption of solute from a liquid solution. The pseudo-first-order kinetic model may be represented by Lagergren:

$$\ln(q_e - q_t) = \ln q_e - k_1 t \quad (9)$$

where q_t is the amount of Fe (III) ions adsorbed ($mg \cdot g^{-1}$) at time t (min) and k_1 is the rate constant of pseudo-first-order adsorption (min^{-1}). The validity of the model can be checked by the linearized plot of $\ln(q_e - q_t)$ versus t . (31, 32); Table 6.

3.11.2. The Pseudo second-order kinetic model

The Pseudo-second-order kinetic model is expressed as:

$$t/q_t = 1/k_2 q_e^2 + t/q_e \quad (10)$$

where the equilibrium adsorption capacity (q_e), and the second order constant k_2 ($g \cdot mg^{-1} \cdot min^{-1}$) can be determined experimentally from the slope and intercept of plot t/q_t versus t (33); Figure 12 and Table 6.

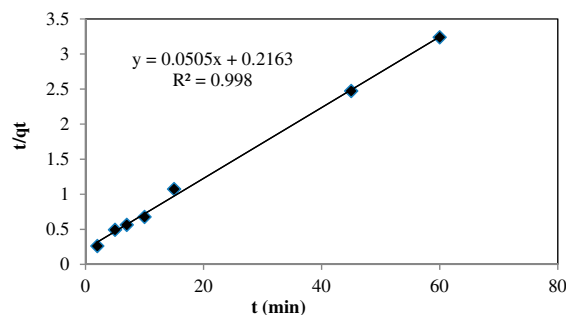


Figure 12. Pseudo-second-order kinetic model.

Table 6. Kinetic parameters.

Kinetic models	parameters	
Pseudo-first-order	q_e (mg. g ⁻¹)	11.61
	k_1 (min ⁻¹)	0.0795
	r^2	0.976
	Δq_t (%)	0.073
Pseudo-second-order	q_e (mg. g ⁻¹)	19.80
	k_2 (min ⁻¹)	0.012
	r^2	0.998
	Δq_t (%)	0.025
Intraparticle kinetic model	K_d (mg. g ⁻¹ . min ^{-1/2})	1.57
	r^2	0.871
	Δq_t (%)	0.36
	β (g. mg ⁻¹)	0.31
Elovich kinetic model	α (mg. g ⁻¹ . min ⁻¹)	18.58
	r^2	0.959
	Δq_t (%)	0.13

3.11.3. Intraparticle diffusion kinetic model

The intraparticle diffusion model is applied to study the adsorption process, which is written as:

$$q_t = k_d \sqrt{t} + C \quad (11)$$

where k_d is intraparticle diffusion rate constant (mg.g⁻¹.min^{-1/2}) (34, 35) and C is the intercept (mg/g) and it gives an idea of the thickness of the boundary layer.

3.11.4. Elovich kinetic model

The Elovich model equation is generally expressed as:

$$q_t = \left(\frac{1}{\beta}\right) \ln(\alpha\beta) + \left(\frac{1}{\beta}\right) \ln t \quad (12)$$

The plot of q_t versus $\ln t$ should yield a linear relationship with a slope $1/\beta$ and an intercept of $1/\beta \ln(\alpha\beta)$ (36). The initial adsorption rate α (mg. g⁻¹. min⁻¹), desorption constant β (g. mg⁻¹), and coefficients of determination (R^2) are given in Table 6.

According to the high correlation ($R^2 = 0.998$ almost equal to unity) and low normalized standard deviation (Δq_t (%) equal to 0.025), the adsorption of Fe (III) ions is best described by the pseudo-second-order kinetic model compared to other kinetic models. Besides, the calculated q_e value ($q_e = 19.80$ mg.g⁻¹) agree with experimental q_e value ($q_{e \text{ exp}} = 18.52$ mg.g⁻¹). These results suggested that the adsorption system studied obeys the pseudo-second-order kinetic model. This

result is in accordance with the findings quoted by other researchers (3, 8, 9, 10).

A comparison of the removal ratio of Fe (III) ions for different adsorbents is given in Table 7. As can be seen, the removal ratio of Fe (III) ions is higher than that of reported adsorbents (3, 10, 37, 38). This result may be due to the effect of surface area, morphology, surface structure, and functional groups. Nonetheless, this comparison is not precise, since the experimental conditions are different.

Conclusion

In this research, manganese oxide nanocomposite (Mn₂O₃/Mn₃O₄) was synthesized by sol-gel method which is a simple and inexpensive technique in the preparation of nanoparticles. Mn₂O₃/Mn₃O₄ nanocomposite was characterized by IR, SEM, and XRD techniques and was used to remove Fe (III) from aqueous solutions. Experiments were conducted as a function of different adsorption parameters (pH of the solution, initial Fe (III) concentration, adsorbent weight, and contact time). RSM by BBD was used to evaluate the effects of four process factors on Fe (III) ions removal. The ANOVA results showed that the pH of the solution and initial Fe (III) concentration were the most significant parameters on the removal ratio Fe (III) ions. In the optimization process, the predicted maximum removal ratio of Fe (III) ions was achieved as 95.80% with a pH of 5, the adsorbent weight of 0.5 g, initial Fe (III) concentration of 50 mg/L, and a contact time of 62.5 min. Equilibrium studies showed that Fe (III) adsorption data follow the Langmuir model. The adsorption kinetic correlated very well with the pseudo-second-order equation. Therefore, it is expected that the Mn₂O₃/Mn₃O₄ nanocomposite with fine grain size (about 48 nm) can be used as one of the effective, convenient, and inexpensive adsorbents for the removal of heavy metals from aqueous solutions.

Acknowledgments

The authors thank the Golestan University for providing financial support for the work described in this paper.

Table 7. The removal ratio of Fe (III) ions by a different type of adsorbents.

Adsorbent	Operating conditions	The removal ratio	Reference
Mn ₂ O ₃ /Mn ₃ O ₄	$W = 0.5$ g/200 ml, $C_0 = 50$ mg/L, $t = 62.5$ min, pH = 5	$\eta = 95.80\%$	This study
Activated carbon from coconut shells (ACCS)	$W = 0.03$ g/100 mL, $C_0 = 20$ mg/L, $t = 60$ min, pH = 5.8	$\eta = 90\%$	(3)
Linde Type A- Zeolite	$W = 0.1$ g/30 mL, $C_0 = 70$ mg/L, $t = 60$ min, pH = 6	$\eta = 96\%$	(10)
Activated carbon	$T = 30-60^\circ\text{C}$, $W = 0.1$ g/50 mL, $C_0 = 50$ mg/L, pH = 2	$\eta = 65\%$	(37)
Aerobic activated sludge	$T = 20^\circ\text{C}$, $W = 0.2$ g/10 mL, $C_0 = 50$ mg/L, $t = 6$ h, pH = 3	$\eta = 65\%$	(38)
Unaerobic activated sludge	$T = 20^\circ\text{C}$, $W = 0.2$ g/100 mL, $C_0 = 50$ mg/L, $t = 6$ h, pH = 3	$\eta = 70\%$	(38)

Disclosure statement

No potential conflict of interest was reported by the authors.

Notes on contributors

Narges Samadani Langeroodi received the Ph.D. degree from Lomonosov Moscow State University, Russian, in 2007. From 2007 to 2018, she worked as assistant professor in department of chemistry at Golestan University. She is currently faculty member in department of chemistry at Golestan University, Iran. Her research interests include surface chemistry, adsorption and methods of reducing or eliminating of pollutants and hazardous materials from the water, kinetics, heterogeneous catalysts and nanoparticles.

Zhaleh Farhadraresh is MSc student at Golestan University, from 2016 to 2018. Her field of study is physical chemistry.

Aliakbar Dehno Khalaji received the Ph.D. degree from Isfahan University of Technology, Iran, in 2007. From 2007 to 2014, he worked as assistant professor in Department of Chemistry at Golestan University. He is currently an associated professor in Department of Chemistry at Golestan University. His research interests include Schiff base complexes, thiosemicarbazones compounds and transition metal oxides nanoparticles.

References

- [1] Han, C.; Pu, H.; Li, H.; Deng, L.; Huang, S.; He, S.; Luo, Y. *J. Hazard. Mater.* **2013**, 254–255, 301–309.
- [2] Hua, M.; Zhang, S.; Pan, B.; Zhang, W.; Lv, L.; Zhang, Q. *J. Hazard. Mater.* **2012**, 211–212, 317–331.
- [3] Moreno-Pirajan, J.C.; Garcia-Cuello, V.S.; Giraldo, L. *Adsorption.* **2011**, 17, 505–514.
- [4] El-Sayed, M.A. *Acc. Chem. Res.* **2001**, 34 (4), 257–264.
- [5] Deliyanni, E.A.; Peleka, E.N.; Matis, K.A. *J. Hazard. Mater.* **2009**, 172, 550–558.
- [6] Mulaudzi, L.Y.; Staden, J.F.V.; van Staden, R.I. *Anal. Chim. Acta.* **2002**, 467, 35–49.
- [7] Aksu, Z.; Calik, A.; Dursum, A.Y.; Demircan, Z. *Process. Biochem.* **1999**, 34, 483–491.
- [8] Bhattacharyya, K.G.; Gupta, S.S. *Adsorption.* **2006**, 12, 185–204.
- [9] Wan Ngah, W.S.; Ab Ghani, S.; Kamari, A. *Biores. Technol.* **2005**, 96, 443–450.
- [10] Hashemian, S.; Hosseini, S.H.; Salehifar, H.; Salari, K. *American J. Analytic. Chem.* **2013**, 4, 123–126.
- [11] Rajasimman, M.; Murugaiyan, K. *J. Adv. Chem. Eng.* **2012**, 2, 1–8.
- [12] Demim, S.; Drouiche, N.; Aouabed, A.; Benayad, T.; Couderchet, M.; Semsari, S.J. *Ind. Eng. Chem.* **2014**, 20, 512–520.
- [13] Kalavathy, H.; Regupathib, M.I.; Pillai, M.G.; Miranda, L.R. *Colloids. Surf. B: Biointerfaces.* **2009**, 70, 35–45.
- [14] Myers, R.H.; Montgomery, D.C.; Anderson-Cook, C.M. *Response Surface Methodology: Process and Product Optimization Using Designed Experiments*, John Wiley & Sons: New York, **2009**.
- [15] Pang, S.C.; Chin, S.F.J. *Nanomater.* **2012**, 2012, 1–7.
- [16] Dhaouadi, H.; Ghodbane, O.; Hosni, F.; Touati, F. *Int. Schol. Res. Netw. (ISRN) Spectrosc.* **2012**, 2012, 1–8.
- [17] Berbenni, V.; Marini, A. *Mater. Res. Bulletin.* **2003**, 38, 1859–1866.
- [18] Oswald, H.R.; Wanpetich, M.J. *Helv. Chim. Acta.* **1967**, 50, 2023–2034.
- [19] Mourabet, M.; Rhilassi, A.E.I.; Boujaady, H.E.I.; Bennani-Ziatni, M.; Hamri, R.E.I.; Taitai, A. *J. Saudi. Chem. Soc.* **2015**, 19, 603–615.
- [20] Montgomery, D.C. *Design and Analysis of Experiments*, 4th ed.; New York: John Wiley & Sons, **2001**.
- [21] Salavati-Niasari, M.; Esmaeili-Zare, M.; Gholami-Daghian, M. *Advance. Powder Technol.* **2014**, 25, 879–884.
- [22] Abareshi, M.; Goharshadi, E.K.; Zebarjad, S.M.; Khandan Fadafan, H.; Yussefi, A. *J. Magn. Mater.* **2010**, 322, 3895–3901.
- [23] Srinivasan, A.; Viraraghavan, T. *J. Hazard. Mater.* **2010**, 175, 695–702.
- [24] Prakash, O.; Talat, M.; Hasan, S.; Pandey, R.K. *Bioresour. Technol.* **2008**, 99, 7565–7572.
- [25] Ma, L.; Peng, Y.; Wu, B.; Lei, D.; Xu, H. *Chem. Eng. J.* **2013**, 225, 59–67.
- [26] Qiu, H.; Lv, L.; Pan, B.-c.; Zhang, Q.-j.; Zhang, W.-m.; Zhang, Q.-x. *J. Zhejiang Univ. Sci. A.* **2009**, 10, 716–724.
- [27] Lagergren, S. *Handlingar.* **1898**, 24, 1–39.
- [28] Ho, Y.S.; McKay, G. *Chem. Eng. J.* **1998a**, 70, 115–124.
- [29] Weber, W.J.; Morris, J.C. *J. Sanit. Eng. Div. Am. Soc. Civ. Eng.* **1963**, 89, 31–60.
- [30] Chien, S.H.; Clayton, W.R. *Soil. Sci. Soc. Am. J.* **1980**, 44, 265–285.
- [31] Ho, Y.S. *Scientometrics.* **2004**, 59, 171–177.
- [32] Ho, Y.S.; McKay, G. *Proc. Safe. Environ. Prot.* **1998b**, 76, 332–340.
- [33] Ho, Y.S.; McKay, G. *Water Res.* **2000**, 34, 735–742.
- [34] Fil, B.A.; Yilmaz, M.T.; Bayer, S.; Elkoca, M.T. *Brazilian. J. Chem. Eng.* **2014**, 31 (01), 171–182.
- [35] Aladag, E.; Fil, B.A.; Boncukcuoglu, R.; Sozudogru, O. *J. Disper. Sci. Technol.* **2014**, 35, 1737–1744.
- [36] Fil, B.A.; Ozmetin, C. *J. Chem. Soc. Pak.* **2012**, 34 (4), 896–906.
- [37] Edwin Vasu, A. *E-J. Chem.* **2008**, 5 (1), 1–9.
- [38] Wu, Y.; Zhou, J.; Wen, Y.; Jiang, L.; Wu, Y.J. *Appl. Biochem. Biotech.* **2012**, 168 (8), 2079–2093.